Pinning/depinning dynamics of trijunction lines during faceted/nonfaceted eutectic growth

S. Mohagheghi, M. Şerefoğlu, Silvère Akamatsu, Sabine Bottin-Rousseau

Pinning/depinning dynamics of trijunction lines during faceted/nonfaceted eutectic growth

S. Mohagheghi[a,1], M. Şerefoğlu[b], S. Akamatsu[c,*], S. Bottin-Rousseau[c]

[a]*Istinye University, Department of Mechanical Engineering, Istanbul, Turkey*
[b]*Marmara University, Department of Metallurgical and Materials Engineering, Maltepe, Istanbul, Turkey*
[c]*Sorbonne Université, CNRS-UMR 7588, Institut des NanoSciences de Paris, case courrier 840, 4 place Jussieu, 75252 Paris Cedex 05, France*

Abstract

We present an in situ experimental study of decoupled- and coupled-growth patterns in a binary faceted/nonfaceted (f/nf) eutectic alloy. Real-time optical observation is carried out at low growth velocity V ($< 0.3\ \mu\mathrm{ms}^{-1}$) during directional solidification of the transparent AminoMethylPropaneDiol-Succinonitrile (AMPD-SCN) eutectic in thin samples. On a large scale, the two-phase growth front mostly exhibits irregularly spaced decoupled-growth patterns involving faceted fiber-like AMPD crystals that protrude in the liquid ahead of, and in weak diffusive interaction with the nonfaceted SCN solid. The morphological stability of low-velocity, steady-state decoupled-growth patterns is evidenced. In addition, three types of (f/nf) coupled-growth patterns with fiber-like, tubular (or "hollow") and C-shaped morphologies, respectively, are identified. New light is cast on the pinning dynamics of trijunctions at which the two solid phases and the liquid meet in equilibrium. A discussion is initiated on the interplay between the interfacial kinetics of the more or less mobile facets and the solute diffusion field, and on the stability of triple junctions with strongly anisotropic interfaces.

Keywords: A1.Directional solidification, A1.Eutectics, A1.Morphological stability, A1.Interfaces

1. Introduction

In many alloys extensively used in industrial applications, a eutectic phase transformation from the undercooled melt leads to the simultaneous growth of two solid phases, one of them being faceted (f), while the other is nonfaceted (nf) [1, 2, 3, 4]. The solidification of such faceted/nonfaceted (f/nf) eutectics leads to the formation of disordered, or "irregular" composite microstructures [5]. Typical examples can be found in metallic systems, such as Al-based alloys with the addition of Si or Ge [6, 7, 8]. Irregular-eutectic solidification microstructures result from a complex growth front dynamics that involves the interplay between solute diffusion in the liquid and a nonlinear attachment kinetics of atoms (or molecules) at the faceted solid-liquid interface. In contrast to the self-organizing dynamics of lamellar and rod-like microstructures in regular eutectics with nonfaceted solid-liquid interfaces [9], the growth of irregular eutectics can be expected to markedly depend on specific properties of the alloy and the crystal structure of the solids. In fact, based on in situ experimental studies, it has been emitted that some remarkable solidification patterns in f/nf eutectics may result from dynamic mechanisms common to a surprisingly large ensemble of systems [4, 8, 10, 11]. In an attempt to provide a clearer classification, new focus has been put on the dynamics of the so-called decoupled- and coupled-growth patterns [8, 10]. In addition to the strongly anisotropic growth kinetics of faceted interfaces, the pinning dynamics of trijunction lines, at which the three phases, namely, the liquid, the nonfaceted solid, and the faceted solid meet in equilibrium, has been recently pointed to being of central importance [10]. However, relevant experimental observations still remain scarce, and clear evidence for the existence and the morphological stability of steady-state f/nf eutectic growth patterns is lacking.

In this paper, we present an in situ experimental study of the dynamics of remarkable f/nf eutectic growth patterns in a transparent irregular-eutectic alloy. In the chosen system, namely the AminoMethylPropaneDiol-

*Corresponding author
Email address: silvere.akamatsu@insp.jussieu.fr (S. Akamatsu)
[1]presently at Access e.V., Intzestr. 5, 52072 Aachen, Germany

Succinonitrile (AMPD-SCN) alloy, two-phase solidification from the liquid involves the essentially pure AMPD and SCN solids [12]. As it is well known, SCN crystals grow nonfaceted from the melt [13]. In contrast, the AMPD solid forms thin fiber(-like) crystals with long (lateral) facets on their sides, which ordinarily do not grow on the scale of the observations (immobile, or "blocked" facets), and mobile facets at their tips [10, 12]. Real-time optical imaging of thin (about 12-μm thick) samples of a near-eutectic AMPD-SCN alloy is carried out during directional solidification at controlled velocity V in a fixed temperature gradient G. Operating at low solidification velocity ($V < 0.3\ \mu\text{ms}^{-1}$) actually permits to observe both decoupled- and coupled-growth patterns devoid of the noncrystallographic branching and impurity effects at higher V in the AMPD-SCN system [10]. We bring experimental evidence for the existence of decoupled- and coupled-growth patterns, and investigate both their formation dynamics and morphological stability in (quasi) steady-state conditions. This provides a unique experimental basis for a better understanding of the physical mechanisms at play in the formation of irregular eutectic growth microstructures in f/nf eutectic alloys. For introductory purposes, "naïve" sketches of decoupled- and coupled-growth patterns, represented in two dimensions, are shown in Fig. 1. They are meant to draw one's attention to important morphological features (to be discussed below) in the region of the three-phase contact: a wet interphase boundary in the solid as concerns the decoupled-growth case (Fig. 1a), and a pinning dynamics of trijunctions with faceted interfaces in coupled-growth f/nf patterns (Fig. 1b).

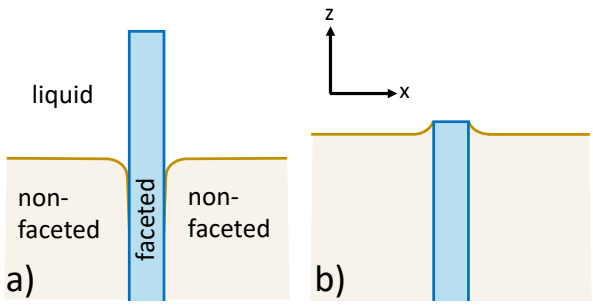

Figure 1: Schematic representations (in two dimensions) of a) decoupled-growth, and b) coupled-growth patterns with faceted fiber crystals aligned with the main solidification axis **z**, during directional solidification of a faceted/nonfaceted eutectic. Color online.

The experimental methods are briefly described in section 2. The main results are presented in section 3. We first report on observations aiming at identifying the basic growth shape of faceted AMPD crystals far from any morphological instability (section 3.1). The central results about decoupled- and coupled-growth patterns are presented in sections 3.2 and 3.3, respectively. Morphological instabilities during initial and transient growth stages are presented in section 3.4. In section 4, we initiate a discussion on the following three points: (1) A decoupled-growth shape is made of a thin faceted crystal, the leading tip of which grows ahead of, i.e., at a higher temperature than the interface between the nonfaceted solid and the liquid (Fig. 1a). Along the blocked facets on the sides of the faceted crystals, no three-phase contact line establishes at, or close to the eutectic temperature T_E. The liquid wets the contact surface between the two solids over a finite temperature range below T_E. (2) In a coupled-growth pattern, the two solids grow essentially at the same temperature, close to T_E (isothermal growth). At the trijunction, the pinning angles (their value in the sketch of Fig. 1b is arbitrary) depend on the anisotropy of the surface free energies of the involved interfaces. (3) On the basis of in situ observations in a transparent organic alloy, an improved description of typical irregular eutectic growth microstructures in many metallic f/nf eutectics based on the dynamics of decoupled- and coupled-growth patterns during directional solidification in thin samples can be achieved.

2. Methods

The binary AMPD-SCN system presents a eutectic point at a temperature $T_E = 325.7$ K [12]. The two (essentially pure) eutectic solids are the body-centered-cubic (bcc) SCN, and the monoclinic AMPD crystal phases. The crystalline parameters of solid AMPD are **a**=0.8621(4), **b**=1.1053(5) and **c**=0.6141(5) nm, and the angle between **a** and **c** is about 93.64° [14]. For an alloy of concentration C_0 close to the eutectic concentration $C_E = 97.4$ mol%SCN, the volume phase fraction of AMPD crystals in the solid is only a few percents. Commercial compounds are purified by multiple distillation/degassing (SCN) and sublimation (AMPD) processes. Slightly hypoeutectic alloys ($C_0 \lesssim C_E$; see section 3.4.1) are prepared by melting and mixing SCN and AMPD in known proportions under argon atmosphere. Thin cartridges are made of two rectangular glass plates separated by thin polyethyleneterephthalate (PET) spacers that fix the thickness of the alloy film to about 12 μm, except otherwise stated. The lateral dimensions of the alloy film are 6×60 mm^2. The

cartridges are filled with the molten alloy under low-pressure argon atmosphere, and sealed after rapid solidification at room temperature. The "as-cast" two-phase microstructure of a sample is usually made of a fine dispersion of small AMPD crystals (with an average diameter typically smaller than 10 μm) in an essentially continuous solid SCN matrix.

The experimental setups and procedures have been presented in detail in previous publications (see, e.g., [10] and [15], and references therein). A thin sample is put in contact with two metallic blocks, separated from each other by a distance set to 5 mm in this study, both equipped with individual heating components and temperature regulations. A uniaxial temperature gradient G (8.0 ± 1.0 Kmm^{-1}) establishes between the two blocks by heat conduction along the sample. We call **z** the axis of the temperature gradient, **x** the (lateral) direction parallel to the isotherms in the sample plane, and **y** the (transverse) direction parallel to the isotherms and perpendicular to the sample plane. Directional solidification (DS) is performed by pulling the sample with a linear motor (PI) toward the cold part of the setup along **z**. In this study, we focus on a low-velocity range ($0.05 \leq V \leq 0.15$ μms^{-1}). The DS setup is mounted on the XYZ stage of an optical microscope, which permits optical scanning of the thin sample over the whole area between the temperature regulated blocks. The growth front is observed in real time in transmitted light. The images (typical field of view: 640×480 μm^2) are recorded with a numerical camera and stored on a computer. Standard image processing (ImageJ software [16]) is used for improving the quality of the images.

3. Results

3.1. Basic growth shape of faceted AMPD crystals

Previous to presenting the dynamics of decoupled- and coupled-growth, we think it is important to focus on the description of the basic growth shape (growth habit) of faceted AMPD crystals. Figure 2a shows two AMPD crystals growing in a decoupled way during a directional-solidification experiment in a 100-μm thick sample. We shall consider the one of the two AMPD crystals (in the middle of the snapshot) which is essentially parallel to (or aligned with) the main growth axis **z**. The lateral size of this aligned crystal (< 30 μm) is smaller than the thickness of the sample. The fiber crystal is not in contact with any of the two sample walls. Its growth is not perturbed by meeting with an inclined AMPD crystal at some distance behind the leading tip. The shape of the aligned AMPD crystal corresponds to a quasi free growth from the liquid, except for the diffusive interaction with the SCN solid matrix at the rear. Therefore it can be considered as a reference growth habit of AMPD fiber crystals from the AMPD-SCN melt.

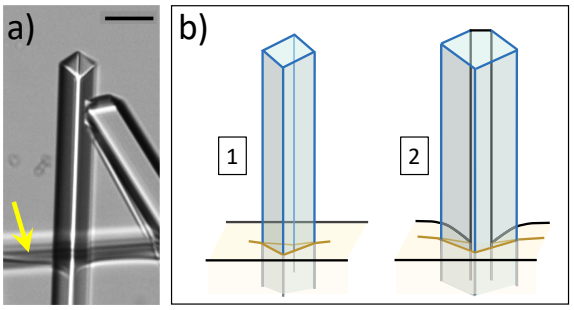

Figure 2: a) Decoupled-growth pattern during directional solidification of a 100-μm thick AMPD-SCN sample. In this image and the following ones, the main solidification axis **z** is vertical (liquid on top). Arrow: SCN-liquid interface. One AMPD crystal is nearly aligned with the **z** axis, the second one strongly tilted. The growth of the latter was stopped by the aligned crystal. $V = 0.1$ μms^{-1}. Bar: 30 μm. b) Schematic representations of decoupled-growth patterns with faceted fiber crystals (1) not contacting, and (2) contacting a sample wall. Blue (yellow): faceted (nonfaceted) crystal. Brown lines: meniscus profile. Black/grey lines: contact lines with the sample walls. Color online.

The observations suggest that the four (blocked) lateral facets of the fiber crystal belong to one and the same family of planes, most probably {110}, of the AMPD monoclinic crystal lattice. Under this assumption, the main growth axis of the AMPD crystal is the [001] direction, which is also the direction of the sharp (within optical resolution) edges delimiting adjacent lateral facets. The small, diamond-shaped facet at the leading tip of the crystal is delimited by sharp edges as well. This "tip facet" is mobile. As made visible in the (side-view) image of Fig. 2a, it is inclined with respect to the isotherms (and it is not perpendicular to the [001] direction) by an angle that is clearly larger than that of the basal (001) plane. however, information is lacking for a precise identification of the tip facet lattice plane. A schematic decoupled-growth pattern (a three-dimensional version of Fig. 1a) reproducing the main morphological features of the experimental image of Fig. 2a is represented in Fig. 2b (sketch 1).

Two additional features are worth mentioning. First, during solidification, the tip of an AMPD crystal actually frequently exhibits several facets, depending on the growth dynamics. This is the case of the tilted AMPD crystal in Fig 2a (also see section 3.4.2). Incidentally, fiber crystals with different tip facet planes have also been observed during growth in the Sn-Cu_6Sn_5 al-

loy [17]. The second point is illustrated in sketch 2 (Fig. 2b), which represents a decoupled-growth pattern with a faceted crystal in contact with one of the glass walls of the sample container. Thicker AMPD crystals can also be in contact with the two sample walls. In addition, AMPD crystals grow most of the time tilted, and make a finite angle from the **z** axis in the **xz** plane parallel to the sample walls (in-plane tilt), and sometimes out of that plane (off-plane tilt). The morphological stability of decoupled-growth patterns with a quasi free-growth configuration, and a faceted crystal presenting a negligible off-plane tilt, will be evidenced in the next section. The in-plane tilt angle of the AMPD crystal can be large (up to more than 50^o). In contrast, decoupled-growth patterns with AMPD crystals presenting a finite off-plane tilt commonly undergo complex morphological instabilities (section 3.4.2).

3.2. Decoupled growth

At a low solidification velocity, the growth of an AMPD-SCN alloy ordinarily presents a decoupled dynamics. A steady-state decoupled-growth pattern is shown in Fig. 3. It was observed to remain morphologically stable over a solidification distance of more than 4 mm (only a part of the microstructure is visible in the figure). In Fig. 3, two AMPD fiber crystals grow tilted, with comparable values of the (slightly diverging) tilt angles (about 17^o for crystal A1 on the left, and 15^o for crystal A2 on the right), which prevents mutual collision. They are separated by a large distance along the growth front (about 270 μm) and are both far away from the other crystals in the sample (outside the field of view of the figure). The SCN-liquid interface presents a slight inward curvature on a large scale, which corresponds to an enrichment of AMPD in the liquid in the median region between two faceted crystals. The apparent widths of the AMPD crystals in Fig. 3 is larger than the nominal thickness of the sample. The crystals are both in contact with at least one of the sample walls, but present a negligible off-plane misalignment. Near an AMPD facet, the SCN-liquid interface forms a meniscus similar to what is observed in a polycrystal near a "wet" grain boundary with a large misorientation angle [18, 19, 20, 21]. There is no trace of any equilibrated trijunction. Qualitatively speaking, the configuration essentially corresponds to that of sketch 2 in Fig. 2b, except for the finite in-plane tilt of the faceted crystals.

Several steady-state decoupled-growth patterns, essentially similar to the case of Fig. 3, were observed during the experiments. This suggests that, during directional solidification of a slightly hypoeutectic

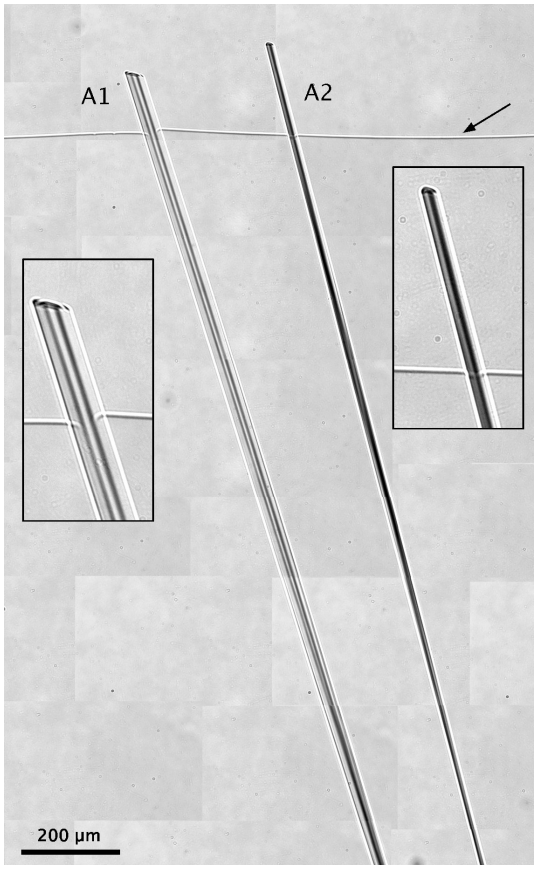

Figure 3: Steady-state decoupled-growth patterns in a thin AMPD-SCN sample ($V = 0.15\ \mu\text{ms}^{-1}$). A1, A2: AMPD crystals. Grayscale variations in the liquid and the SCN solid matrix are an image-processing artifact (collage of several individual snapshots). Insets: double-scale images of the two faceted AMPD fiber crystals growing tilted ahead of the smooth SCN-liquid interface (arrow).

AMPD-SCN alloy at sufficiently low velocity, steady-state decoupled-growth patterns are morphologically stable.

Let us add two observations in support to the latter statement. The first one corresponds to the dynamics, illustrated in Fig. 4a, of decoupled-growth patterns involving very thin fiber crystals that grow tilted in a convergent way. In that case, in contrast to Fig. 2a, the two AMPD crystals cross each other in the thickness of the sample, without direct contact, and continue to grow without substantial interaction or detectable shape change. The second observation was made during the solidification of an AMPD-SCN alloy in a 350-μm thick sample (Fig. 4b), that is, in a three-dimensional geometry quite representative of bulk solidification. In that case, a large number of decoupled-growth patterns with different orientations of the AMPD crystals grow in a stable way –collisions of AMPD crystals with a neighboring one or a sample wall are rare events. In conclusion, at low solidification velocity, decoupled-growth patterns are intrinsically stable, and their lifetime is determined by the collective dynamics of tilted faceted crystals, and the interactions with the sample walls.

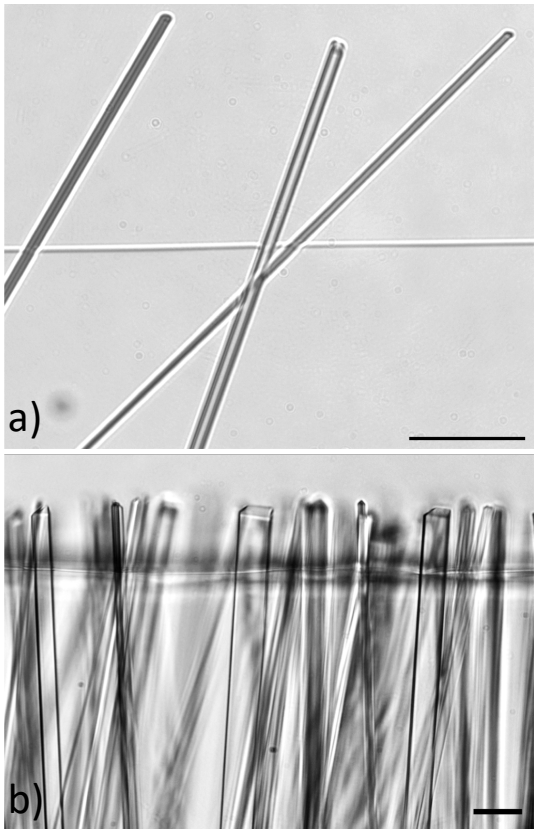

Figure 4: Decoupled-growth patterns. a) Thin sample. Three AMPD fiber crystals grow tilted. Two of them crossed each other in the thickness of the sample during growth. $V = 0.15\ \mu\mathrm{ms}^{-1}$. b) Thick sample (thickness: 350 μm). Some of the AMPD crystals are out of focus. $V = 0.05\ \mu\mathrm{ms}^{-1}$. Bars: 100 μm.

3.3. Coupled growth

Three types of coupled-growth patterns, representative of experimental observations made in thin AMPD-SCN samples at low solidification velocity, are shown in Fig. 5. The first one (Fig. 5a) involves a tilted AMPD crystal that contacts with at least one of the sample walls, probably the two ones. The tip facet of the AMPD crystal is significantly inclined with respect to the central axis of the crystal. The coupled-growth pattern is markedly asymmetric: a trijunction is pinned at the lower edge of the crystal tip, on the front side of the pattern (with respect to the lateral drift of the tip) –hence the "one-sided" appellation given to this type of coupled-growth pattern. The trijunction oscillates, thus leaving a striated trace in the solid. No trijunction is observed on the rear side, and an SCN-liquid meniscus forms at a slightly lower temperature than the trijunction.

The second type of coupled-growth pattern is shown in Fig. 5b. The main feature is a "tubular" growth, with a thin SCN rod crystal occupying the core of the faceted AMPD crystal. Tubular growth shapes are also called "hollow" structures in the scientific literature in reference to an apparent axial "void" that is left after applying selective chemical etching to metallic eutectics (see, e.g., Refs. [22, 23, 24, 25]). The formation process of such a tubule in the AMPD-SCN eutectic system is shown in Fig. 6. Initially, the dynamics is decoupled,

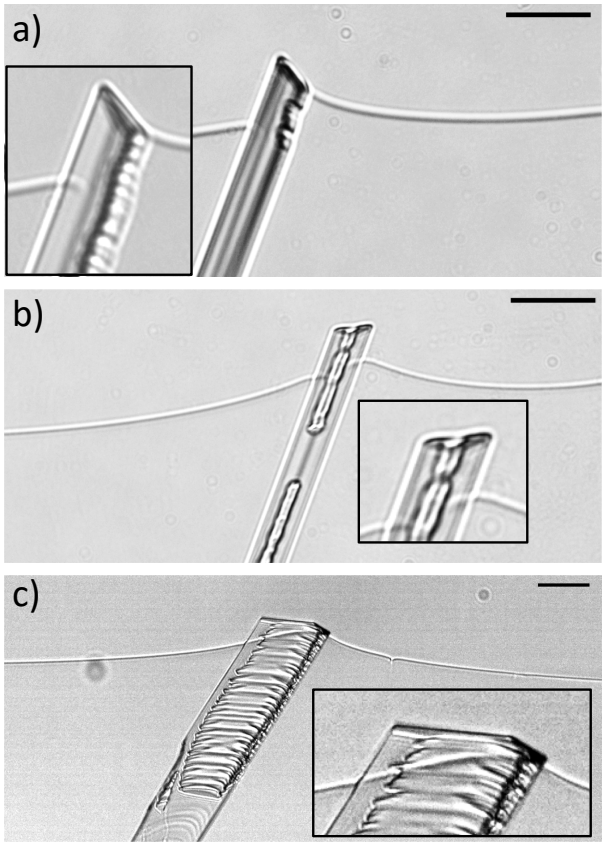

Figure 5: Coupled-growth patterns in thin AMPD-SCN samples. a) One-sided pattern ($V = 0.05\ \mu\mathrm{ms}^{-1}$). Inset: 1.5×-magnified detail of the same pattern at a later time. b) Tubular pattern ($V = 0.15\ \mu\mathrm{ms}^{-1}$). Inset: 1.7×-magnified detail. c) C-shaped pattern ($V = 0.05\ \mu\mathrm{ms}^{-1}$). Inset: 2.2×-magnified detail. Bars: 50 μm.

and the AMPD crystal tip grows very close to, but at a finite distance from the SCN solid (Fig. 6a). At a certain time, the SCN-liquid interface accelerates and reaches the tip facet (Fig. 6b). The contact is very brief, and breaks up within a few seconds (Fig. 6c). The main SCN-liquid interface recoils back to its former position, but a small SCN crystal is deposited in the center of the AMPD crystal tip, and grows in a coupled way, in the shape of an axial rod inside the AMPD crystal (Fig. 6d). This tubular coupled-growth morphology is weakly stable, and the inner SCN crystal rod is prone to intermittent pinching off, thus resulting in an interrupted-tubule microstructure as shown in Fig. 5b.

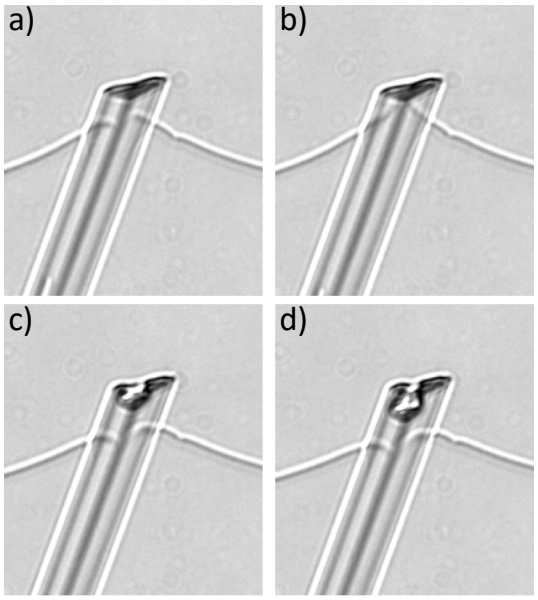

Figure 6: Formation of a tubular coupled-growth pattern. a) Initial decoupled-growth pattern. b) Pinning of a trijunction. c) Depinning of the trijunction. d) Tubular proceeds with coupled growth at the tip of the AMPD crystal. $V = 0.15\ \mu\mathrm{ms}^{-1}$. Time interval between each image: 30 s. Horizontal dimension of each panel: 100 μm.

The third type of coupled-growth pattern is shown in Fig. 5c. The AMPD crystal is strongly tilted. It is oriented in such a way that one of the lateral facets is nearly parallel to the sample wall, with, however, a slight off-plane misalignment. The SCN solid grows between that facet and one of the glass plates (the SCN-liquid interface is visible in transparency in Fig. 5c). The AMPD crystal has a relatively large lateral extension, and two mobile facets can be identified at the tip. The main, remarkable feature is the concave shape of the faceted crystal. It is likely that the space left between the AMPD crystal and the glass plate is filled with an SCN crystal. A trijunction line, hardly visible in the image, runs

along the edge of the tip facet, more or less parallel to the glass plate, and is slightly curved towards the interior of the AMPD crystal. The cross-section of the faceted crystal can be described as an elongated "C" shape (also see, e.g., Refs. [26] and [27]). In this C-shaped coupled-growth pattern, as in the one-sided and tubular coupled-growth patterns described above, the trijunction line oscillates, and the interphase boundary in the solid is striated.

In this section and in section 3.2 above, we have brought strong experimental evidence for the existence of (quasi) steady-state coupled- and decoupled-growth patterns, respectively, during directional solidification of the f/nf eutectic AMPD-SCN system. In the following section, we report observations of transient mechanisms, some of them leading to the formation of the various patterns, some others limiting their morphological stability.

3.4. Transient stages and morphological instabilities

3.4.1. Initial transient

It is of common knowledge that determining crystal selection processes occur during the initial stages of a directional-solidification experiment [1, 28]. In the present work, at the start of an experiment, a thin AMPD-SCN sample, once placed in the solidification setup, undergoes a partial directional melting. Figure 7a shows the typical structure of a sample at the end of an annealing time (of about 20 min) at rest ($V = 0$) in the temperature gradient. The unmelted solid on the cold side presents an as-cast two-phase microstructure. The homogenous liquid on the hot side is clearly seen at the top of the image. In an intermediate layer, small AMPD crystals remain dispersed in the liquid. These AMPD crystals are thus the primary phase, that is the alloy is actually slightly hypoeutectic. During annealing, a slow, but incomplete coarsening of the AMPD crystals is observed. Along the axis of the temperature gradient, the two-phase (AMPD-liquid) region extends between $z = z_E$ (at $T = T_E$) and z_1 ($> z_E$), the latter corresponding to a temperature T_1 close to the liquidus temperature $T^{liquidus}$ of the AMPD-liquid equilibrium [28].

When the solidification is started ($V > 0$), the AMPD crystals hardly grow and recoil along $\mathbf{z}$ –in this paper, the term "recoil" designates a decrease in the z position of a given interface over time. Since SCN has almost no solubility in the solid AMPD phase (vanishing partition coefficient), a quasi linear recoil of the AMPD crystal layer at the beginning of the solute redistribution transient is indeed expected [29]. The nonfaceted SCN grows through the incomplete AMPD layer. Most

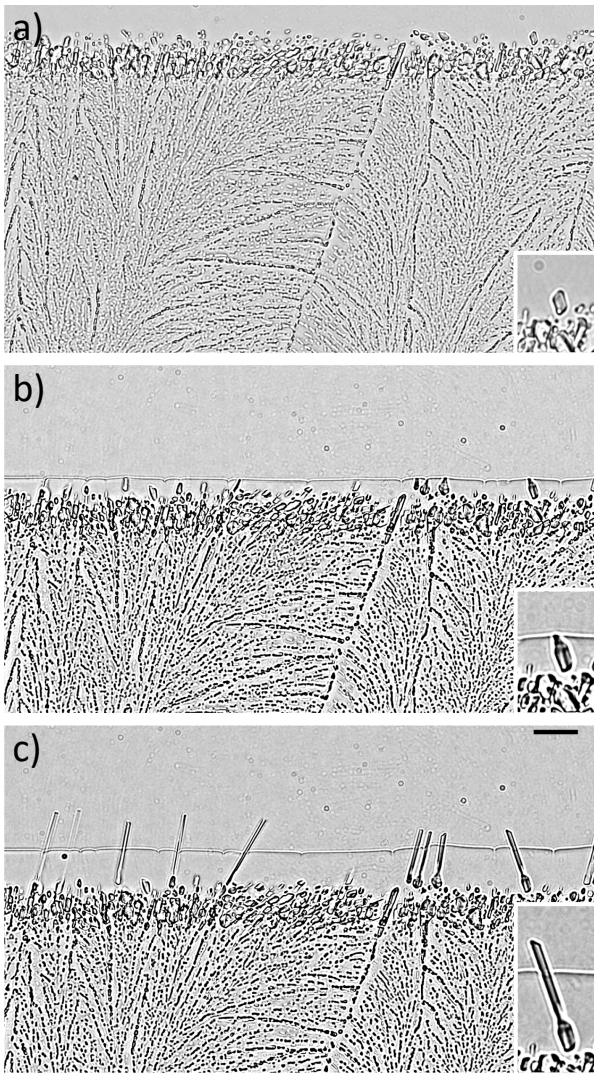

Figure 7: Directional solidification of a slightly hypoeutectic AMPD-SCN alloy in a thin sample (initial stages). a) End of annealing ($V = 0$). b) Early stages of the solidification: transient coupled growth a short time (about 11 min) after V has been set to 0.15 μms^{-1}. c) Onset of decoupled growth about 4 min later. Bar: 100 μm. Some optical artifacts in the liquid region could not been removed. Insets: large-magnification details showing (a) an AMPD crystal in the liquid, (b) a transient AMPD-SCN coupling and (c) decoupled growth of the very same crystal.

of the AMPD crystals are encapsulated by the SCN solid, except for a few of them, which locally form coupled-growth structures (Fig. 7b). The z position of the coupled-growth front in Fig. 7b is 40−50 μm below z_E in Fig. 7a. This shift, which corresponds to an apparent temperature difference of less than 0.5°C, can actually be attributed to an instrumental "advection" of the temperature diffusion field toward the cold side of the directional-solidification bench (thermal recoil), unavoidably associated to the translation motion of the sample [29]. No effect due to residual impurities was observed.

During the coupled-growth stage, the AMPD crystals undergo a dramatic thinning. Some of them are pinched-off, in particular those with a substantial off-plane misalignment. After a short time lapse, the mobile tips of the remaining faceted crystals detach from the SCN solid and grow rapidly in the liquid. This instability gives rise to a fully decoupled-growth regime (Fig. 7c) with AMPD fiber crystals protruding ahead of the SCN-liquid interface. Thin faceted crystals with a very strong in-plane tilt are also rapidly eliminated. After a while, the distance between the AMPD tips and the SCN-liquid interface stabilizes, and the decoupled-growth regime reaches steady-state. By taking the thermal recoil into account, a comparison between the three panels of Fig. 7 informs us that (i) the position of the AMPD crystal tips remains below $T^{liquidus}$, as expected, and (ii) the temperature of the SCN-liquid interface, including the menisci at the contact of the immobile facets of the AMPD crystals, is substantially below T_E.

The severe selection mechanism of AMPD crystals during the early stages of solidification, and the low mobility of the lateral facets (which prevents easy splitting) entail that, at least at low solidification velocity, the actual volume phase fraction of the AMPD phase in the solid is lower than that predicted by the equilibrium phase diagram. The distance between two neighbor AMPD crystals is large, the liquid remains rich in AMPD solute, and the average temperature of the SCN-liquid interface is well below T_E. These features, in addition to those directly associated to the highly anisotropic growth of the faceted crystals, contrast with those of regular, nonfaceted eutectics.

3.4.2. Precursory instability

In this section and in the following one, we investigate specifically how decoupled growth can become unsteady at low velocity in thin samples. As it has been illustrated in Fig. 2a, a converging-growth process can lead to the arrest of a tilted AMPD crystal due to meeting with a neighboring crystal of large thickness. This leads to the elimination of some of the AMPD crystals that were selected during the initial stages of solidification, thus contributing to a decrease of the AMPD volume fraction in the solid.

Figure 8a shows a more complex phenomenon. It involves a decoupled-growth pattern with an AMPD crystal that presents a negligible in-plane tilt, which facilitates the observation over long times, but a slight off-plane misalignment –it grows in contact with, and towards one of the sample walls. Between times t_0 and t_1, the cross-section of the crystal decreases, and the area of the AMPD-glass contact surface increases. Two of the lateral facets eventually disappear (time t_2). Just after time t_2, one of the surviving lateral facets suddenly becomes mobile, and the AMPD crystal thickens. Simultaneously, the SCN solid grows along the (transiently) mobile facet of the AMPD crystal (time t_3), and a curved trijunction line forms. A faintly contrasted striation of the interphase boundary in the solid (time t_4 panel of Fig. 8a) signals an oscillatory instability of the trijunction (see section 3.3). A second facet with a slower growth kinetics appears at the tip (time t_3) and the initial facet shrinks until elimination (time t_4). The new facet tip recoils, but remains at a finite distance ahead of the SCN-liquid interface. In this case, the trijunction eventually becomes unstable (see the trace left in the solid; time t_5), and the lateral AMPD facet becomes immobile (blocked) again. In the images, the inclination of the long edges between the blocked facets does not change: the process does not involve any detectable distortion of the AMPD crystal.

In Fig. 8b, the z positions z_{tip} and z_{SCN} of the AMPD crystal tip and the SCN-liquid interface, respectively, at fixed x values (see inset) are plotted as a function of time t. The recoil of the SCN-liquid interface between times t_0 and t_2 signals an increase of the AMPD concentration in the melt. This is consistent with the thinning (i.e., the decrease of volume) of the AMPD crystal. The non-monotonous variation of z_{tip} between t_0 and t_2 may be due to changes in both the kinetics of the tip facet and the diffusion field, as well as the variation of the geometry of the AMPD crystal. The steep decrease of z_{tip} after time t_2 corresponds to the appearance of the slow-growth facet at the tip. The increase of z_{SCN} as soon as the trijunction forms is clearly visible in the graph. After depinning of the trijunction, z_{SCN} again decreases.

In summary, the evolution of the AMPD-SCN pattern described above involves the appearance of a new facet at the tip, a transient mobility of a lateral facet, and the pinning of a trijunction line along that facet, at a finite distance at the rear of the tip facet. Several mechanisms operate on a scale that is not accessible optically.

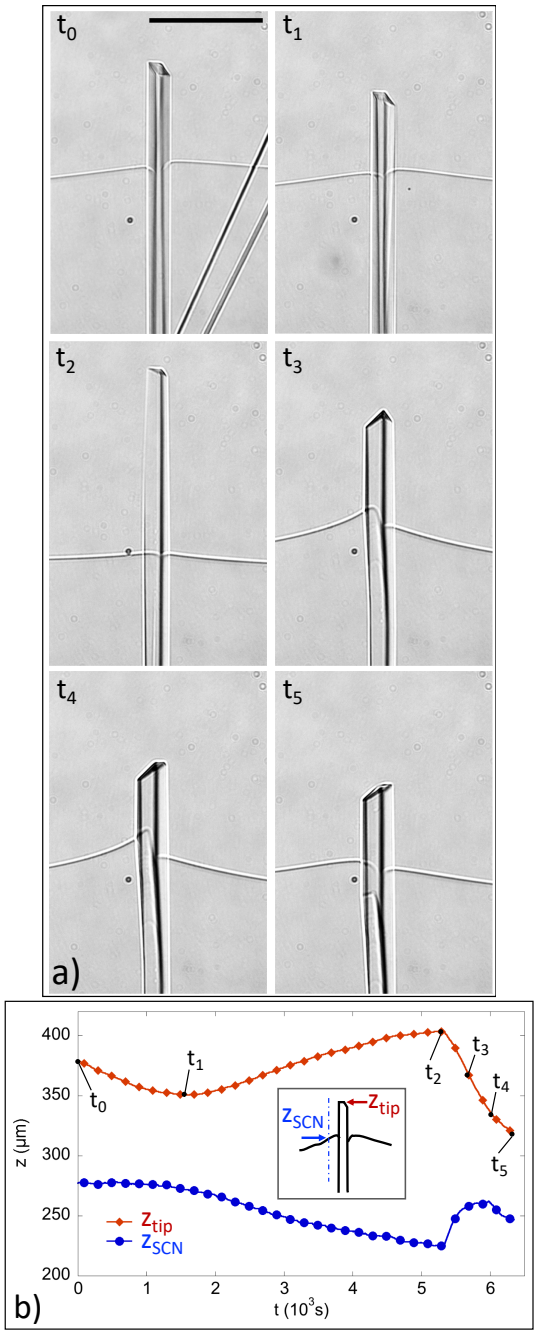

Figure 8: a) Decoupled-growth pattern at six different times (t_0 = 0, t_1 = 28, t_2 = 88, t_3 = 96, t_4 = 100, t_5 = 106 min). $V = 0.15\ \mu\text{ms}^{-1}$. Bar: 100 μm. b) Position along **z** of the tip of the AMPD crystal (z_{tip}), and of the SCN-liquid interface (z_{SCN}) as a function of time t (see the schematic drawing in the inset). Lines are mere guides for the eye.

The interaction of the AMPD crystal with the glass wall most probably leads to the appearance of a microscopic defect at an edge of the contact surface, which serves as a source of elementary steps that propagate along the faceted AMPD-liquid interface. The AMPD-liquid interface is then no longer an atomically smooth facet, but a mobile, vicinal surface with a finite dynamic roughness [18]. This makes possible the pinning of a trijunction line, the shape and the stability of which depends critically on how the step-flow source operates. In the present case, the system is eventually driven back to an ordinary decoupled-growth regime. In some other occurrences, as shown in the next section, it serves as a precursor to the formation of coupled-growth patterns.

3.4.3. Formation of a coupled-growth pattern

We could observe the formation of coupled-growth patterns as part of a large-scale decoupled-growth dynamics at low solidification velocity. In Fig. 9, many features can be understood under the light of the observations reported in the previous sections. First, as in Fig. 4a, several events involving the crossing of thin converging AMPD crystals in the thickness of the sample can be seen. Second, as illustrated in Fig. 2a, the growth of a tilted AMPD crystal can be terminated when it encounters a thick crystal with a cross section comparable to the thickness of the sample. Third, the thickening instability of the AMPD crystal labelled C1 on the left side of the panels (Figs. 9c and 9d) is similar to that described in the previous section.

In a first stage, the evolution of the strongly tilted AMPD crystal C2 (Figs. 9a and 9b) is more or less similar to that of crystal C1. However, the SCN-liquid interface presents a large deformation (Fig. 9b), the distance $z_{tip} - z_{SCN}$ (same notations as in Fig. 8) decreases continuously, and the SCN-liquid interface eventually reaches an edge of crystal C2 (Fig. 9c). In contrast to Fig. 8, the process leads to the formation of a long-lived coupled-growth pattern (Fig. 9d). The C-shaped coupled-growth pattern of Fig. 5c formed in comparable circumstances. As mentioned above, the formation of coupled-growth patterns at low solidification velocity is favored by the interaction of the AMPD crystals with the glass plates. It is thus expected to be relatively less frequent in bulk samples. This remains to be confirmed via a more systematic study in thick samples.

3.4.4. Splitting instability

One-sided coupled-growth patterns (Fig. 5a) are observed to be stable over long solidification times, except when they are subjected to a finite perturbation (for example after a change of the solidification velocity by

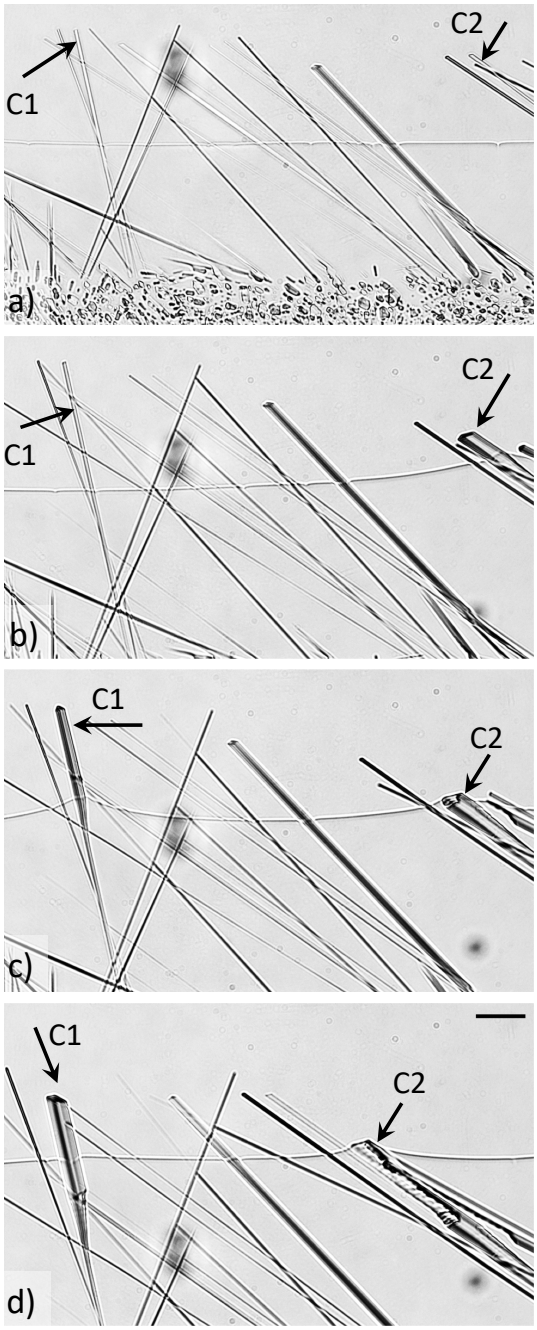

Figure 9: Large-scale growth dynamics in a thin AMPD-SCN sample at different times after solidification was started (time $t = 0$): a) 40 min; b) 46 min; c) 58 min; and d) 73 min. C1 and C2: two AMPD crystals of particular interest (see text). $V = 0.10\ \mu\text{ms}^{-1}$. Bar: 50 μm.

the operator or due to an interaction with a thick, converging AMPD crystal). As mentioned above, tubular patterns (Fig. 5b) are basically intermittent, and prone to pinching-off.

The dynamics of C-shaped patterns is more complex. These patterns are often observed to widen in the lateral direction (the C-like shape becomes more and more elongated). This widening process almost systematically leads to a splitting instability, which most often gives rise to two (or more) separate decoupled-growth patterns, as illustrated in Fig. 10. In some instances (inset in Fig. 10), a hybrid (coupled/decoupled-growth) pattern forms after splitting. Importantly, the AMPD crystals originating from a splitting instability are systematically observed to grow parallel to each other, in crystallographic continuity with the parent crystal. In other words, in the AMPD-SCN system, the splitting instability at low solidification velocity preserves the orientation of the faceted crystals. As in the case of the transient instability presented in section 3.4.2, it does not involve any measurable plastic deformation, in contrast to the non-crystallographic branching that was observed at larger V [10].

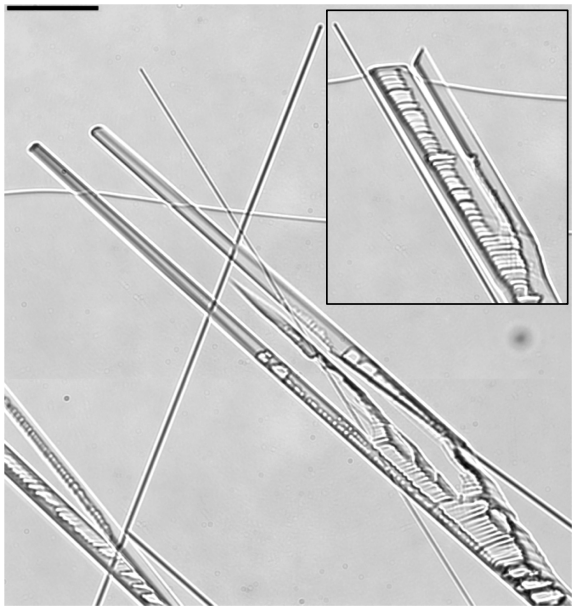

Figure 10: Solidification pattern and microstructure resulting from a splitting instability of a C-shaped coupled-growth pattern: formation of two separate decoupled-growth patterns (a third branch, in between the two surviving AMPD crystals, was eliminated). $V = 0.1\ \mu\text{ms}^{-1}$. Bar: 100 μm. Inset: splitting instability leading to a hybrid pattern ($V = 0.05\ \mu\text{ms}^{-1}$). Same space scale.

It is tempting to make a comparison of the splitting of a large C-shaped coupled-growth pattern with the lamel-

lar or rod splitting instability in regular-eutectic arrays. However, the latter leads to an adjustment of the interphase spacing in a basically periodic eutectic growth structure. Here, the splitting instability affects a single coupled-growth pattern with a C-shaped AMPD crystal that gets wide enough. The splitting dynamics shown in Fig. 10 probably involves a complex interplay between the diffusion field, the growth kinetics of facets, and the pinning dynamics of the trijunction line. No splitting instability was observed during decoupled growth at low solidification velocity.

4. Discussion

The schematic f/nf eutectic growth shapes presented in Fig. 11 are proposed to capture the main morphological features of the decoupled- and coupled-growth patterns observed during the directional solidification of thin AMPD-SCN samples at low solidification velocity. We discuss their relevance to a larger class of irregular eutectics.

Decoupled growth. A generic decoupled-growth pattern is represented in Fig. 11a with a tilted faceted crystal. The (single) facet at the tip, which is drawn with an arbitrary inclination angle, connects the blocked facets with sharp edges. The interfaces between the nonfaceted solid and the liquid on the two sides of the faceted crystal are represented with (i) a large-scale inward curvature, thus accounting for the long-range interplay with the diffusion field in the liquid, and (ii) a small convex meniscus close to the blocked solid-liquid facets on the sides of the fiber crystals. The interphase boundaries in the solid run in continuity with, and parallel to the blocked facets. They are most probably wetted by a microscopically thin liquid layer [20, 21], as stated in section 3.2. Decoupled-growth patterns have been observed in various other systems, in particular during directional solidification of an Sn-Ni_3Sn_4 alloy (Fig. 5 in Ref. [4]), and an Al-Si alloy (Fig. 16b in Ref. [6]). The resemblance between the latter (observed in a longitudinal section after a rapid quench) and our observations in the AMPD-SCN system is striking. The fact that Si crystals grow in the form of thin platelets seems of secondary importance, and the 2D representation in Fig. 11a is essentially justified. A schematic cross-section of the microstructure left in the solid by a decoupled-growth pattern is shown as an inset in Fig. 11a. It presents the same facets as those of the solid-liquid growth habit of AMPD crystals. A platelet-like shape could be also shown for more general purposes.

Let us add a few remarks. It was shown in section 3.4.2 that, at low velocity, decoupled-growth pat-

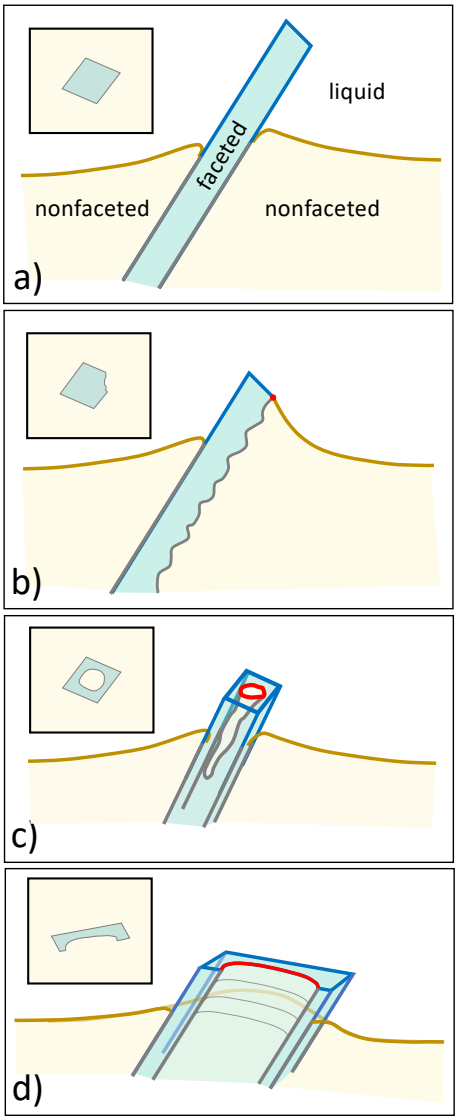

Figure 11: Schematic representation of f/nf eutectic growth patterns at low solidification velocity. a) Decoupled growth. b), c) and d): One-sided, tubular, and C-shaped coupled-growth patterns, respectively. In a) and b), a two-dimensional geometry is drawn, for simplicity. In b), c) and d), the trijunction is represented in red. The two solids are designated as nonfaceted and faceted, respectively. Insets: schematic cross-sections of the resulting microstructures in the solid. Color online.

terns can become unstable when being in contact with a sample wall. The key phenomenon in this case is the transient mobility of one of the lateral (ordinarily blocked) facets. We took advantage of this process to observe coupled-growth patterns at low solidification velocity. In a previous work [10], it was shown that, in the AMPD-SCN system, coupled growth prevails when V is increased. This can be understood by considering the variation of the temperature difference $\delta T = T_{tip} - T_{SCN}$ between the faceted tip (T_{tip}) and the SCN-liquid interface (T_{SCN}) as a function of V. In the AMPD-SCN system, T_{tip} decreases when V increases, as expected for faceted growth. In comparison, T_{SCN} does not depend much on V. In other words, δT decreases when V increases, and vanishes at a critical velocity V_c, above which coupled growth becomes favorable. In the AMPD-SCN system, the value of V_c was estimated to about 0.3 μms^{-1} [10]. However, as it can be seen in Fig. 9, T_{tip}, and thus the actual value of V_c, depend on the inclination angle of the AMPD crystals. In addition, in the AMPD-SCN system, coupled growth at $V > V_c$ also goes along with frequent non-crystallographic branching [10], that is, the growth of new crystals with a small, but finite misorientation from the parent ones [30], making the dynamics highly unsteady. Focusing on very low solidification velocities allowed us to explore both decoupled- and coupled-growth patterns in the absence of those phenomena.

A theoretical (or numerical) approach aiming at establishing the existence of steady-state decoupled-growth patterns and their stability may be at hand. A challenging task would be to determine how the diffusion field in the liquid around the faceted crystal and the interfacial kinetics at the tip contribute to the selection of steady-state f/nf decoupled-growth patterns and their stability, as well as the dependence of δT on V.

Coupled growth. Schematic one-sided, tubular, and C-shaped coupled-growth patterns are represented in Fig. 11b, 11c and 11d, respectively. Their main differences stem from the shape and the position of the trijunction line. In Fig. 11b, the sketched one-sided coupled-growth pattern provides a 2D version of the experimental pattern of Fig. 5a –the trijunction thus appears as a mere point. More symmetric coupled-growth shapes comparable to Fig. 1b were not observed in steady-state, but during very short transient stages such as that of Fig. 7b. This may be due to the large inclination, and the specific interfacial kinetics of the tip facets of AMPD crystals. The existence of symmetric coupled-growth patterns (Fig. 1b) in a less anisotropic system still remains to be evidenced. In a tubular pattern (Fig. 11c), the trijunction is a closed loop, more or less centered at the tip of the faceted crystal. The schematic C-shaped pattern of Fig. 11d is simplified as compared to the image of Fig. 5c –in particular, the tip of the faceted crystal presents a single facet.

In this study, tubular and C-shaped microstructures are observed to be related with coupled growth and the pinning dynamics of a trijunction line. On the experimental side, the use of a transparent system, and the real-time visualization of the various interfaces on a micrometer scale have proven decisive. Theoretically, the local equilibrium of surface tension vectors at the trijunction is described by the Young-Herring equation [31]. In the present cases, the nonfaceted SCN-liquid interface, which can be considered as essentially isotropic, meets the two strongly anisotropic SCN-AMPD and AMPD-liquid interfaces. This presents an additional complexity as compared to the so-called locked-lamellar patterns in regular-eutectic grains with anisotropic interphase boundaries in the solid, but isotropic solid-liquid interfaces [32]. However, it is worth noticing that close to the trijunction, the interphase boundary in the solid is concave, and therefore looses its faceted character. It is no longer parallel to the blocked solid-liquid facet, which makes a noticeable difference with decoupled growth. It can be emitted that the wavy, or striated shape of the interphase boundary results from an oscillatory dynamics of the trijunction, and can be attributed to (i) a strong sensitivity of the pinning angles to the least rotation of markedly anisotropic interfaces near the trijunction (thus to slight perturbations in the system), and (ii) the existence of forbidden (or Herring unstable) inclinations in the anisotropic Wulff shapes. This is also reminiscent of the so-called kinks in locked-lamellar eutectic grains (nonfaceted eutectics) [33, 34, 35]. The more or less stable dynamics of a trijunction involving strongly anisotropic interfaces –pinning/depinning events, oscillatory motion– is likely to be generic to a large ensemble of coupled-growth patterns in f/nf eutectics. The formation of micro-facets, and a slightly unsteady balance between interfacial kinetics and the diffusion field can further complexify the phenomenon [36].

Finally, not only faceted fibers and platelets, but also tubular (or hollow) [22, 23, 24, 25] and C-shaped [26, 27] microstructures have been frequently observed in solidified f/nf eutectic alloys. However, very few explanations have been provided on their formation mechanisms based on unambiguous, in situ observations during near steady-state directional solidification. Tubular and C-(or L-)shaped growth morphologies of AMPD crystals in a substantially off-eutectic AMPD-SCN sam-

ple were shown in Ref. [12], without any details being given on their formation dynamics. In Ref. [24], considering an essentially isothermal solidification of an Sn-Cu alloy, it was suggested that a hollow-like shape might form via a partial, dislocation driven remelting of the core of faceted fiber crystal. In both cases, however, the nonfaceted phase is expected to eventually grow along or inside a concave region of the interface between the liquid and the faceted solid. This, again, must involve a transient coupled-growth stage, and a pinning/depinning dynamics of trijunctions, which was directly monitored in the present study.

5. Conclusion

The real-time evolution of decoupled- and coupled-growth patterns has been observed in situ during thin-sample directional solidification of a transparent, faceted/nonfaceted eutectic alloy at low velocity. Strong experimental evidence has been brought in support to two main statements, namely, the existence of stable steady-state decoupled-growth patterns, and the role of the pinning dynamics of three-phase junction lines (trijunctions) in the formation and the stability of coupled-growth patterns. Close similarities of the growth patterns in the transparent system with remarkable fiber, tubular and C-shaped microstructures, which are common in irregular-eutectic alloys, have been highlighted. We insist that the real-time visualization of the dynamics of trijunction lines on a micrometer scale, made possible in a transparent system, is a key contribution of the present work to a better understanding of irregular eutectics.

Several questions remain open. Sub-micrometer mechanisms (step flow along facets, pinning/depinning motions of the trijunctions) that govern the instability from faceted fibers to tubular and C-shaped crystals cannot be resolved optically. On a larger scale, the long-term dynamics of decoupled- and coupled-growth patterns with tilted faceted crystals in bulk samples has not been much explored. It could also be worth studying the evolution of this dynamics as a function of important parameters that were kept unchanged in this study, such as the value of the temperature gradient, and the concentration of the alloy –as well as the thickness of the samples. More interestingly, in the present system, the morphological transition from decoupled to coupled growth, that is, the establishment of an isothermal growth of the two solid phases with a stable trijunction, does not change radically the irregular character of the solidification regime. It should be interesting to explore other systems, such as the Al-Al_3Ni eutectic, which present a morphological transition from irregular to regular (rod-like) microstructures at relatively low solidification velocities (on the order of 10 μms^{-1}) [37]. The present study could give precious information for guiding such an investigation, as well as carrying out a theoretical and/or numerical investigation of steady-state patterns with partly faceted solid-liquid interfaces.

ACKNOWLEDGMENTS

We gratefully acknowledge Maria Achache for technical help. This work was funded by the bilateral program between TUBITAK (Grant No. 217M089) and Campus France (PHC BOSPHORUS 39706RE).

References

[1] J. A. Dantzig, M. Rappaz, Solidification, 2nd Edition, EPFL Press, Lausanne (2016).
[2] W. Kurz, D.J. Fisher, M. Rappaz, Fundamentals of Solidification, Trans Tech Publications, Zürich, Switzerland (2022).
[3] D. A. Pawlak, S. Turczynski, M. Gajc, K. Kolodziejak, R. Diduszko, K. Rozniatowski, J. Smalc, Irina Vendik, How far are we from making metamaterials by self-organization? The microstructure of highly anisotropic particles with an SRR-like geometry, Adv. Funct. Mater. 20 (2010) 1116-1124.
[4] N. Hou, S. A. Belyakov, L. Pay, A. Sugiyama, H. Yasuda, C. M. Gourlay, Competition between stable and metastable eutectic growth in Sn-Ni alloys, Acta Mater. 149 (2018) 119-131.
[5] J.D. Hunt, K.A. Jackson, Binary eutectic solidification, Trans. Metall. Soc. AIME 236 (1966) 843-852.
[6] A. Hellawell, The growth and structure of eutectics with silicon and germanium, Prog. Mater. Sci. 15 (1970) 3-78.
[7] T. Hosch, LG England, R.E. Napolitano, Analysis of the high growth-rate transition in Al-Si eutectic solidification, J. Mater. Sci. 44 (2009) 4892-4899.
[8] A. J. Shahani, X. Xiao, P. W. Voorhees, The mechanism of eutectic growth in highly anisotropic materials, Nat. Commun. 7 (2016) 12953.
[9] K. A. Jackson, J. D. Hunt, Lamellar and rod eutectic growth, Trans. Metall. Soc. AIME 236 (1966) 1129-1142.
[10] S. Mohagheghi, S. Bottin-Rousseau, S. Akamatsu, M. Şerefoğlu, Decoupled versus coupled growth dynamics of an irregular eutectic alloy, Scr. Mater. 189 (2020) 11-15.
[11] N. Hou, J.W. Xian, A. Sugiyama, H. Yasuda, C.M. Gourlay, Ag_3Sn Morphology Transitions During Eutectic Growth in Sn–Ag Alloys, Metall. Mater. Trans. A 54A (2023) 909-927.
[12] V. T. Witusiewicz, L. Sturz, U. Hecht, S. Rex, Thermodynamic description and unidirectional solidification of eutectic organic alloys: IV. Binary systems neopentylglycol–succinonitrile and amino-methyl-propanediol–succinonitrile, Acta Mater. 53 (2005) 173-183.
[13] S. C. Huang, M.E. Glicksmann, Overview 12: Fundamentals of dendritic solidification—I. Steady-state tip growth, Acta Metall. 29 (1981) 701-715.
[14] J. Salud, D. O. López, M. Barrio, J. Ll. Tamarit, H. A. J. Oonk, P. Negrier, Y. Haget, On the crystallography and thermodynamics in orientationally disordered phases in two-component systems, J. Solid State Chem. 133 (1997) 536-544.

[15] S. Akamatsu, S. Bottin-Rousseau, M. Perrut, G. Faivre, V.T. Witusiewicz, L. Sturz, Real-time study of thin and bulk eutectic growth in Succinonitrile-(D)Camphor alloys, J. Cryst. Growth 299 (2007) 418.
[16] C. A. Schneider, W.S. Rasband, K.W. Eliceiri, NIH Image to ImageJ: 25 years of image analysis, Nat. Methods 9 (2012) 671-675.
[17] J.W. Xian, S.A. Belyakov, K. Nogita, H. Yasuda, C.M. Gourlay, Faceted and Nonfaceted Growth of Cu6Sn5 Crystals, Solidification Processing 2017: Proceedings of the 6th Decennial International Conference on Solidification Processing, ed. Z. Fan (2017) 251-254.
[18] D.P. Woodruff, The solid-liquid interface, Cambridge University Press, Cambridge (1973).
[19] R. Kikuchi, J.W. Cahn, Grain-boundary melting transition in a two-dimensional lattice-gas model, Phys. Rev. B 21 (1985) 1893.
[20] R.J. Schaefer, M.E. Glicksman, J.D. Ayers, High-confidence measurement of solid-liquid surface-energy in a pure material, Phil. Mag. 32 (1975) 725.
[21] S. Ghosh, A. Karma, M. Plapp, S. Akamatsu, S. Bottin-Rousseau, G. Faivre, Influence of morphological instability on grain-boundary trajectory during directional solidification, Acta Mater. 175 (2019) 214-221.
[22] K.S. Kima, S.H. Huha, K. Suganuma, Effects of intermetallic compounds on properties of Sn–Ag–Cu lead-free soldered joints, J. Alloys Compd. 352 (2003) 226-236
[23] S. Ma, J. Xing, Y. He, Y. Li, Z. Huang, G. Liu, Q. Geng, Microstructure and crystallography of M7C3 carbide in chromium cast iron, Mater. Chem. Phys. 161 (2015) 65-73
[24] J.W. Xian, S.A. Belyakov, M. Ollivier, K. Nogita, H. Yasuda, C.M. Gourlay, Cu6Sn5 crystal growth mechanisms during solidification of electronic interconnections, Acta Mater. 126 (2017) 540-551.
[25] S. Chen, X. Mi, G. Huang, Y. Li, Effect of Ce addition on microstructure and properties of Cu–Zn–Mn– Al–based alloy, Mater. Res. Express 6 (2019) 016518.
[26] M. Kaczkan, D.A. Pawlak, S. Turczyński, M. Malinowski, Emission properties of (SrTiO3-TiO2):Pr3+ eutectic with self-organized fractal microstructure, Optical Materials 33 (2011) 1519-1524.
[27] S. K. Aramanda, K. Chattopadhyay, A. Choudhury, Exotic three-phase microstructures in the ternary Ag-Cu-Sb eutectic system, Acta Mater. 221 (2021) 117400.
[28] S. Akamatsu, S. Moulinet, G. Faivre, The formation of lamellar eutectic grains in thin samples, Metall. Mater. Trans. A 32 (2001) 2039-2048.
[29] S. Akamatsu, G. Faivre, Residual-impurity effects in directional solidification: Long-lasting recoil of the front and nucleation-growth of gas bubbles, J. Phys. I France 6 (1996) 503-527.
[30] J. Bisault, G. Ryschenkow, G. Faivre, Spherulitic branching in the crystallization of liquid selenium, J. Cryst. Growth 110 (1991) 889-909.
[31] D. W. Hoffman, J. W. Cahn, Vector thermodynamics for anisotropic surfaces. 1. Fundamentals and application to plane surface junctions, Surf. Sci. 31 (1972) 368-388.
[32] S. Akamatsu, S. Bottin-Rousseau, M. Şerefoğlu, G. Faivre, A theory of thin lamellar eutectic growth with anisotropic interphase boundaries, Acta Mater. 60 (2012) 3199-3205.
[33] B. Caroli, C. Caroli, G. Faivre, J. Mergy, Lamellar eutectic growth of CBr_4-C_2Cl_6: effect of crystal anisotropy on lamellar orientations and wavelength dispersion, J. Cryst. Growth 118 (1992) 135-150.
[34] S. Akamatsu, S. Bottin-Rousseau, M. Şerefoğlu, G. Faivre, Lamellar eutectic growth with anisotropic interphase boundaries: Experimental study using the rotating directional solidification method, Acta Mater. 60 (2012) 3206-3214.
[35] S. Mohagheghi, M. Şerefoğlu, Quasi-isotropic and locked grain growth dynamics in a three-phase eutectic system, Acta Mater. 151 (2018) 432-442.
[36] J.D. Hunt, D.T.J. Hurle, The structures of faceted/nonfaceted eutectics, Trans. Metall. Soc. AIME 242 (1968) 1043-1047.
[37] Y.X. Zhuang, X.M. Zhang, L.H. Zhu, Z.Q. Hu, Eutectic spacing and faults of directionally solidifed Al-Al3Ni eutectic, Sci. Technol. Adv. Mater. 2 (2001) 37-39.